AIMS Mathematics, 11(11): 37355–37376.
DOI:10.3934/math.20261445
Received: 29 June 2026
Revised: 29 October 2026
Accepted: 06 November 2026
Published: 11 November 2026

https://www.aimspress.com/journal/Math

Research article

Modeling the dominant period of infectious disease: The effect of human dispersal in a coupled two-patch SIS model

Hong Yang* **and Fenfen Zhang**

School of Mathematics and Statistics, Taiyuan Normal University, Jinzhong 030619, Shanxi, China

* **Correspondence:** Email: yanghong_9002@163.com.

Abstract: Infectious diseases continue to pose a grave threat to humanity. Beyond uncontrollable factors like climate change and viral evolution, understanding the effect of human mobility on the infectious disease's dominant period is of great significance. In this study, we develop a two-patch SIS model with demographic dynamics using a Markov modeling approach. By applying the Fourier transform, we derive the power spectral density of the infected population. Model parameters are estimated by fitting the model to influenza data from Beijing and Shanghai for the period 2004–2018. Our numerical results demonstrate that the diffusion rate only generates a dominant period for influenza within a specific parameter range. Furthermore, a nonlinear relationship exists between the diffusion rate and the dominant period under specific parameter values: As the diffusion rate increases, the dominant period initially decreases before increasing, yet the above results depend on the model structure and the parameter values.

Keywords: two-patch SIS model; power spectral density; diffusion rate; dominant period; influenza
Mathematics Subject Classification: 92D30, 65C30, 92C42

1. Introduction

Rapid advancements in transportation have facilitated fast population mobility, making the cross-regional spread of infectious disease increasingly prevalent [1, 2]. Infectious disease models [3–5] are instrumental in capturing the effects of this mobility on disease transmission. These models can be classified along several axes: By methodology into continuous and discrete models [6]; by the nature of movement into Eulerian (for location-based perspectives) [7] and Lagrangian (for individual-based tracking) models [8]; by spatial scale into two-patch [9] and multi-patch (or metapopulation) models [10, 11]; and by the inclusion of randomness into deterministic and stochastic frameworks [12]. A primary focus of these models is the basic reproduction number (R_0), particularly the qualitative influence of the dispersal rate on R_0. However, they often fall short of delivering quantitative

characterizations of this effect.

China's complex topography and climatic influences result in diverse periodic patterns of infectious disease (such as influenza) [13, 14]. Describing this phenomenon with deterministic models requires incorporating periodic transmission rates [15, 16] or inducing a Hopf bifurcation [17], which imposes stringent model requirements. A key limitation of this approach is that the resulting oscillations are typically confined to a single fixed frequency, failing to capture the varied periodic patterns across different regions. Stochastic models, however, offer a more parsimonious explanation [18–20]. They can generate oscillations [21, 22] even when the underlying deterministic system has only a stable equilibrium, thus providing a better framework for explaining the multi-periodic behavior observed in infectious disease.

Wavelet analysis [23–25] and the Fourier transform are both effective tools for frequency-domain analysis of noisy data, but they are suited for different types of signals: Wavelet analysis for non-stationary data and the Fourier transform for stationary data. Applying this to the steady-state solution of the epidemic model, the Fourier transform can be employed to derive the power spectral density (PSD). This allows for the identification of the system's dominant frequency and the quantitative characterization of how various factors influence it. For instance, [26] utilized this approach to attribute the 2-8-year cycle of outbreaks of avian influenza primarily to environmental viruses. Similarly, [27] examined the relationship between the population's contact number (degree) and the infection frequency.

The rest of the paper is organized as follows. In Section 2, we develop a stochastic model by deriving the mean and covariance for a two-patch SIS model that incorporates demographic dynamics using a Markov modeling approach. In Section 3, by linearizing the system around the endemic equilibrium and applying the Fourier transform, the PSD of the infected population in both patches is derived. In Section 4, we utilize influenza data from Beijing and Shanghai to compute the dominant period, allowing us to examine the relationship between the diffusion rate and the dominant period. In Section 5, the paper summarizes our findings, acknowledges its limitations, and proposes directions for future work.

2. Markov stochastic modeling process

Compared with that of deterministic models, the prediction of stochastic models is not a single deterministic value but a probability distribution, and the sensitivity to any particular initial condition is correspondingly reduced. Compared with other stochastic modeling approaches, the Markov modeling framework adopted here can directly accommodate discrete state variables and imposes fewer restrictions on the form of the randomness, such as non-Gaussian and jump-type stochasticity. Moreover, a richer set of analytical tools is available for the transition probability matrix. In this paper, the population N is divided into two classes: S and I, where S denotes the number of individuals who are susceptible to disease but are not yet infected; I represents the number of those who are infected with the disease and are able to transmit the disease to susceptible people by coming into contact with them. At the same time, the population N can be divided into N_1 and N_2 according to the patch in which individuals are located, with $N_1 + N_2 = N$. Then the whole population can be divided into 4 compartments: S_1, S_2, I_1, and I_2; $S_1 + I_1 = N_1$ and $S_2 + I_2 = N_2$.

Let $X = (S_1, I_1, S_2, I_2)^{tr}$, $\Delta X = (\Delta S_1, \Delta I_1, \Delta S_2, \Delta I_2)^{tr}$, and let $p(\Delta\delta = \delta' - \delta|\delta)$ denote the rate at

which the system changes state from δ to δ', resulting in a change of $\Delta\delta$. e_j is the standard unit vector in R^4. The number of individuals belonging to each compartment changes in time due to the following processes: Infection, recovery, dispersal, birth, and death. According to the infinitesimal transition probabilities summarized in Table 1, the change in the random variable X caused by an event occurring at time t can be expressed as follows:

Infection in patch j: S_j may become infected by contact with an infected individual, i.e., $S_j \overset{\beta_j S_j \frac{I_j}{N_j}}{\rightarrow} I_j$, where β_j is the infection rate ($j = 1, 2$). Then this transition process can be written as

$$p\{(\Delta S_j(t), \Delta I_j(t)) = (-1, +1) | (S_j(t), I_j(t)) = (S_j, I_j)\} = \beta_j \frac{S_j I_j}{S_j + I_j} \Delta t + o(\Delta t). \tag{2.1}$$

Recovery in patch j: Infective people can become susceptible as they recover, $I_j \overset{\gamma_j}{\rightarrow} S_j$, where γ_j is the recovery rate. This transition process can be denoted as

$$p\{(\Delta S_j(t), \Delta I_j(t)) = (+1, -1) | (S_j(t), I_j(t)) = (S_j, I_j)\} = \gamma_j I_j \Delta t + o(\Delta t). \tag{2.2}$$

Dispersal: Bidirectional dispersal of both susceptible and infected individuals between the two patches is allowed. Susceptible and infective people from patch k can move to patch j and vice versa. d^S_{kj} represents the dispersal rate of susceptible individuals from patch k to patch j, and d^I_{kj} has a similar meaning ($k = 1, 2, k \neq j$). These transition processes can be denoted as

$$\begin{aligned}
p\{(\Delta S_j(t), \Delta S_k(t)) = (+1, -1) | (S_j(t), S_k(t)) = (S_j, S_k)\} &= d^S_{kj} S_k \Delta t + o(\Delta t),\\
p\{(\Delta S_j(t), \Delta S_k(t)) = (-1, +1) | (S_j(t), S_k(t)) = (S_j, S_k)\} &= d^S_{jk} S_j \Delta t + o(\Delta t),\\
p\{(\Delta I_j(t), \Delta I_k(t)) = (+1, -1) | (I_j(t), I_k(t)) = (I_j, I_k)\} &= d^I_{kj} I_k \Delta t + o(\Delta t),\\
p\{(\Delta I_j(t), \Delta I_k(t)) = (-1, +1) | (I_j(t), I_k(t)) = (I_j, I_k)\} &= d^I_{jk} I_j \Delta t + o(\Delta t).
\end{aligned} \tag{2.3}$$

Birth in patch j: Newly born individuals are all susceptible, which results in an increase in the number of susceptible individuals, i.e., $S_j \overset{u_j N_j}{\rightarrow} S_j + 1$, where u_j is the birth rate. This transition process can be denoted as

$$p\{\Delta S_j(t) = +1 | S_j(t) = S_j\} = u_j N_j \Delta t + o(\Delta t). \tag{2.4}$$

Death in patch j: Suppose the death rate equals the birth rate. Similar to the above transition process, this process can be denoted as

$$\begin{aligned}
p\{\Delta S_j(t) = -1 | S_j(t) = S_j\} &= u_j S_j \Delta t + o(\Delta t),\\
p\{\Delta I_j(t) = -1 | I_j(t) = I_j\} &= u_j I_j \Delta t + o(\Delta t).
\end{aligned} \tag{2.5}$$

The complete system of δ and $\Delta\delta$ is 4-dimensional. Here, the notation is simplified, and only the varying quantities are written out. For example, because of a new infection in patch 1, the random variable $X(t) = (S_1(t), I_1(t), S_2(t), I_2(t))^{tr}$ changes to $X(t + \Delta t) = (S_1(t + \Delta t), I_1(t + \Delta t), S_2(t + \Delta t), I_2(t + \Delta t))^{tr}$, leading to $\Delta X = X(t + \Delta t) - X(t) = (-1, +1, 0, 0)^{tr} = -e_1 + e_2$.

In addition to these 26 changes in (2.1)–(2.5), there is also the possibility of no change, $\Delta X = \mathbf{0}^{tr}$, whose probability of occurrence is one minus the sum of these 26 probabilities. These 27 probabilities account for all of the possible changes in time Δt, i.e., their probabilities sum to 1, $\sum_{i=1}^{27} p(\delta' - \delta = \Delta X_i | \delta) = 1$.

2.1. Stochastic differential equation model

Under the sparsity assumption that the probability of more than one event occurring in a small interval Δt is $o(\Delta t)$, the number of occurrences of each event type is approximately Poisson distributed over Δt, so that its mean equals its variance. Under the assumptions of mutual independence among events, the Markov (memoryless) property, and path continuity, superposing the mean and covariance contributions of all events listed in Table 1 yields the drift and diffusion (stochastic) terms of the corresponding stochastic differential equation. Based on the transition probabilities in Table 1, the expectation and covariance for the changes in the two patches are computed. The expectation, $E(\Delta t) = \sum_{i=1}^{27} p(\delta' - \delta = \Delta X_i|\delta)\Delta X_i$ is a 4×1 vector. To order Δt, the expectation can be expressed as follows:

$$E(\Delta t) = M\Delta t = \begin{pmatrix} u_1N_1 - u_1S_1 - \frac{\beta_1 S_1 I_1}{N_1} + \gamma_1 I_1 - d_{12}^S S_1 + d_{21}^S S_2 \\ \frac{\beta_1 S_1 I_1}{N_1} - (u_1 + \gamma_1)I_1 - d_{12}^I I_1 + d_{21}^I I_2 \\ u_2N_2 - u_2S_2 - \frac{\beta_2 S_2 I_2}{N_2} + \gamma_2 I_2 + d_{12}^S S_1 - d_{21}^S S_2 \\ \frac{\beta_2 S_2 I_2}{N_2} - (u_2 + \gamma_2)I_2 + d_{12}^I I_1 - d_{21}^I I_2 \end{pmatrix} \Delta t.$$

Table 1. Infinitesimal transition probabilities for the stochastic two-patch model.

Description	Transition	Probabilities
Infection in patch j	$S_j \to S_j - 1$, $I_j \to I_j + 1$	$\beta_j S_j \frac{I_j}{N_j}\Delta t + o(\Delta t)$
Recovery in patch j	$S_j \to S_j + 1$, $I_j \to I_j - 1$	$\gamma_j I_j \Delta t + o(\Delta t)$
Healthy dispersal from patch k to j	$S_k \to S_k - 1$, $S_j \to S_j + 1$,	$d_{kj}^S S_k \Delta t + o(\Delta t)$
Healthy dispersal from patch j to k	$S_k \to S_k + 1$, $S_j \to S_j - 1$,	$d_{jk}^S S_j \Delta t + o(\Delta t)$
Infected dispersal from patch k to j	$I_k \to I_k - 1$, $I_j \to I_j + 1$	$d_{kj}^I I_k \Delta t + o(\Delta t)$
Infected dispersal from patch j to k	$I_k \to I_k + 1$, $I_j \to I_j - 1$	$d_{jk}^I I_j \Delta t + o(\Delta t)$
Healthy birth in patch j	$S_j \to S_j + 1$	$u_j N_j \Delta t + o(\Delta t)$
Healthy death in patch j	$S_j \to S_j - 1$	$u_j S_j \Delta t + o(\Delta t)$
Infected death in patch j	$I_j \to I_j - 1$	$u_j I_j \Delta t + o(\Delta t)$

In addition, the covariance matrix associated with these changes is a 4×4 matrix, $\Sigma(\Delta X) = E([\Delta X][\Delta X]^{tr}) - E(\Delta X)[E(\Delta X)]^{tr}$, which to order Δt is approximately $\Sigma(\Delta X) = E([\Delta X][\Delta X]^{tr}) = \sum_{i=1}^{27} p(\delta' - \delta = \Delta X_i|\delta)\Delta X_i(\Delta X_i)^{tr} = B\Delta t$, in which $B = (b_{u,v})_{4\times4}$ is a symmetric matrix ($u, v = 1, ..., 4$), and

the upper triangular entries of the matrix are listed as follows:

$$b_{ii} = \begin{cases} u_m I_m + \dfrac{\beta_m S_m I_m}{S_m + I_m} + \gamma_m I_m + d_{12}^S S_1 + d_{21}^S S_2, & i = 2m-1, (m = 1, 2), \\ \dfrac{\beta_m S_m I_m}{S_m + I_m} + (\gamma_m + u_m) I_m + d_{12}^I I_1 + d_{21}^I I_2, & i = 2m, \end{cases}$$

$b_{12} = -\frac{\beta_1 S_1 I_1}{N_1} - (\gamma_1 + u_1) I_1$, $b_{34} = -\frac{\beta_2 S_2 I_2}{N_2} - (\gamma_2 + u_2) I_2$, $b_{13} = -d_{12}^S S_1 - d_{21}^S S_2$, $b_{24} = -d_{12}^I I_1 - d_{21}^I I_2$, $b_{14} = b_{23} = 0$.

Then the corresponding stochastic differential equation that models this stochastic process can be written:

$$\begin{aligned} \mathrm{d}X(t) &= M(X(t), t)\mathrm{d}t + \mathrm{d}\eta(t), \\ \langle \eta_u(t) \rangle &= 0, \langle \eta_u(t)\eta_v(t') \rangle = b_{uv}\delta(t - t'), \end{aligned} \tag{2.6}$$

in which η denotes white noise containing $4 * 1$ elements, i.e., $\eta = (\eta_1, \eta_2, \eta_3, \eta_4)^{tr}$.

2.2. Linear stochastic differential equation

For the stochastic differential equation, its deterministic part is expressed as:

$$\frac{\mathrm{d}X(t)}{\mathrm{d}t} = M(X(t), t). \tag{2.7}$$

The reproduction number R_0 of (2.7) can be determined by applying the methodology proposed in [28, 29]. $R_0 = \rho(FV^{-1})$ is the spectral radius of the matrix FV^{-1}, in which

$$F = \begin{pmatrix} \beta_1 & 0 \\ 0 & \beta_2 \end{pmatrix}, V = -\begin{pmatrix} -u_1 - \gamma_1 - d_{12}^I & d_{21}^I \\ d_{12}^I & -u_2 - \gamma_2 - d_{21}^I \end{pmatrix}.$$

Set

$$\begin{aligned} h_1 &= \beta_1 - u_1 - \gamma_1 - d_{12}^I + \beta_2 - u_2 - \gamma_2 - d_{21}^I, \\ h_2 &= (u_1 + \gamma_1 + d_{12}^I - \beta_1)(u_2 + \gamma_2 + d_{21}^I - \beta_2) - d_{12}^I d_{21}^I. \end{aligned}$$

Then $R_0 = \frac{h_1 + \sqrt{h_1^2 - 4h_2}}{2} + 1$. The qualitative analysis of the deterministic equation (2.7) has been conducted in [9]. Accordingly, we shall only list the pertinent conclusions in this work.

Theorem 2.1. *If $R_0 < 1$, the disease-free equilibrium $E_0 = \left(\frac{d_{21}^S N}{d_{21}^S + d_{21}^S}, 0, \frac{d_{12}^S N}{d_{21}^S + d_{21}^S}, 0\right)$ of* (2.7) *is globally stable. If $R_0 > 1$, then the disease is uniformly persistent in the two patches, i.e., a positive equilibrium E_* always exists for system* (2.7).

Our primary focus is on the behavior near the positive equilibrium point. By the theorem above, for $R_0 > 1$, linearization about this point leads to the following Langevin equation:

$$\begin{aligned} \mathrm{d}X(t) &= AX(t)\mathrm{d}t + \mathrm{d}\eta(t), \\ \langle \eta_u(t) \rangle &= 0, \langle \eta_u(t)\eta_v(t') \rangle = b_{uv}|_{E_*}\delta(t - t'), \end{aligned} \tag{2.8}$$

in which $A = (a_{uv}) = \frac{\partial M}{\partial X}|_{E_*}$ is the Jacobian matrix of M with respect to X around E_*.

3. Power spectrum

We use the convention $\tilde{X}(w) = \int_{-\infty}^{+\infty} X(t)e^{iwt}\mathrm{d}t$, where i is the imaginary unit. Since

$$\begin{aligned}
\int_{-\infty}^{+\infty} \dot{X}\, e^{i\omega t}\,\mathrm{d}t &= [\, Xe^{i\omega t}\,]\Big|_{-\infty}^{+\infty} - \int_{-\infty}^{+\infty} X\,\mathrm{d}e^{i\omega t} = -i\omega\,\tilde{X}(\omega),\\
\langle \tilde{\eta}_u(\omega)\,\tilde{\eta}_v(\omega')\rangle &= \iint_{-\infty}^{+\infty} \langle \eta_u(t)\,\eta_v(t')\rangle\, e^{i\omega t}\, e^{i\omega' t'}\, dt\, dt'\\
&= b_{uv}\big|_{E_*} \int_{-\infty}^{+\infty} e^{i(\omega+\omega')t}\, dt\\
&= 2\pi\, b_{uv}\big|_{E_*}\, \delta(\omega+\omega'),
\end{aligned}$$

taking the Fourier transform of (2.8) gives

$$\begin{aligned}
-iw\tilde{X}(w) &= A\tilde{X}(w) + \tilde{\eta}(w),\\
<\tilde{\eta}_u(w)\tilde{\eta}_v(w') > &= 2\pi b_{uv}|_{E_*}\delta(w+w').
\end{aligned} \tag{3.1}$$

By applying Cramer's rule, the solution to the aforementioned system of linear equations (3.1) can be determined. In light of our focus on the results concerning the infected population, we report only the results for I_1 and I_2:

$$\begin{aligned}
\tilde{I}_1 &= \frac{-(iw)^3\tilde{\eta}_2 + (iw)^2C_{11} + (iw)C_{12} + D_{12}\tilde{\eta}_1 + D_{22}\tilde{\eta}_2 + D_{32}\tilde{\eta}_3 + D_{42}\tilde{\eta}_4}{D(w)},\\
\tilde{I}_2 &= \frac{-(iw)^3\tilde{\eta}_4 + (iw)^2C_{21} + (iw)C_{22} + D_{14}\tilde{\eta}_1 + D_{24}\tilde{\eta}_2 + D_{34}\tilde{\eta}_3 + D_{44}\tilde{\eta}_4}{D(w)},
\end{aligned} \tag{3.2}$$

where

$$\begin{aligned}
C_{11} &= a_{21}\tilde{\eta}_1 + a_{23}\tilde{\eta}_3 + a_{24}\tilde{\eta}_4 - (a_{11}+a_{33}+a_{44})\tilde{\eta}_2,\\
C_{12} &= a_1\tilde{\eta}_1 + b_1\tilde{\eta}_2 + c_1\tilde{\eta}_3 + d_1\tilde{\eta}_4,\\
C_{21} &= a_{41}\tilde{\eta}_1 + a_{42}\tilde{\eta}_2 + a_{43}\tilde{\eta}_3 - (a_{11}+a_{22}+a_{33})\tilde{\eta}_4,\\
C_{22} &= a_2\tilde{\eta}_1 + b_2\tilde{\eta}_2 + c_2\tilde{\eta}_3 + d_2\tilde{\eta}_4,\\
a_1 &= a_{21}a_{33} + a_{21}a_{44} - a_{23}a_{31} - a_{24}a_{41},\\
b_1 &= a_{13}a_{31} + a_{14}a_{41} + a_{34}a_{43} - a_{11}a_{33} - a_{11}a_{44} - a_{33}a_{44},\\
c_1 &= a_{11}a_{23} + a_{23}a_{44} - a_{13}a_{21} - a_{24}a_{43},\\
d_1 &= a_{11}a_{24} + a_{24}a_{33} - a_{14}a_{21} - a_{23}a_{34},\\
a_2 &= a_{22}a_{41} + a_{33}a_{41} - a_{21}a_{42} - a_{31}a_{43},\\
b_2 &= a_{11}a_{42} + a_{33}a_{42} - a_{12}a_{41} - a_{32}a_{43},\\
c_2 &= a_{11}a_{43} + a_{22}a_{43} - a_{13}a_{41} - a_{23}a_{42},\\
d_2 &= a_{12}a_{21} + a_{13}a_{31} + a_{23}a_{32} - a_{22}a_{33} - a_{11}a_{22} - a_{11}a_{33},
\end{aligned}$$

D_{uv} is the inverse of the algebraic complement of the corresponding element A_{uv} of the matrix A, and the denominator is given by

$$D(w) = w^4 - i(trA)w^3 - \Omega_1 w^2 + i\Omega_2 w + \det A,$$

where trA denotes the trace of A and $\det A$ means the value of the determinant of A, and Ω_1 and Ω_2 are the sums of all the second-order and third-order principal minors of A, respectively.

Averaging the squared moduli of $\tilde{I}_1$ and $\tilde{I}_2$ gives the power spectra

$$\begin{aligned} P_1(w) &= \langle|\tilde{I}_1|^2\rangle = 2\pi\frac{b_{22}w^6 + \Lambda_{11}w^4 + \Lambda_{12}w^2 + \Lambda_{13}}{|D(w)|^2}, \\ P_2(w) &= \langle|\tilde{I}_2|^2\rangle = 2\pi\frac{b_{44}w^6 + \Lambda_{21}w^4 + \Lambda_{22}w^2 + \Lambda_{23}}{|D(w)|^2}, \end{aligned} \tag{3.3}$$

in which

$$\begin{aligned} \Lambda_{11} =& a_{21}^2 b_{11} + 2(a_1 - a_{11}a_{21} - a_{21}a_{33} - a_{21}a_{44})b_{12} + 2a_{21}a_{23}b_{13} + 2a_{21}a_{24}b_{14} \\ &+ (a_{11}^2 + 2a_{11}a_{33} + 2a_{11}a_{44} + a_{33}^2 + 2a_{33}a_{44} + a_{44}^2 + 2b_1)b_{22} \\ &+ 2(c_1 - a_{11}a_{23} - a_{23}a_{33} - a_{23}a_{44})b_{23} + a_{23}^2 b_{33} + 2a_{23}a_{24}b_{34} + a_{24}^2 b_{44} \\ &+ 2(d_1 - a_{11}a_{24} - a_{24}a_{33} - a_{24}a_{44})b_{24}, \\ \Lambda_{12} =& (a_1^2 - 2D_{12}a_{21})b_{11} + 2(D_{12}a_{11} + D_{12}a_{33} + D_{12}a_{44} - D_{22}a_{21} + a_1 b_1)b_{12} \\ &+ 2(a_1 c_1 - D_{12}a_{23} - D_{32}a_{21})b_{13} + 2(a_1 d_1 - D_{12}a_{24} - D_{42}a_{21})b_{14} \\ &+ (2D_{22}a_{11} + 2D_{22}a_{33} + 2D_{22}a_{44} + b_1^2)b_{22} + (d_1^2 - 2D_{42}a_{24})b_{44} \\ &+ 2(D_{32}a_{11} + D_{32}a_{33} + D_{32}a_{44} - D_{22}a_{23} + b_1 c_1)b_{23} + (c_1^2 - 2D_{32}a_{23})b_{33} \\ &+ 2(D_{42}a_{11} + D_{42}a_{33} + D_{42}a_{44} - D_{22}a_{24} + b_1 d_1)b_{24} \\ &+ 2(c_1 d_1 - D_{32}a_{24} - D_{42}a_{23})b_{34}, \\ \Lambda_{13} =& D_{12}^2 b_{11} + 2D_{12}D_{22}b_{12} + 2D_{12}D_{32}b_{13} + 2D_{12}D_{42}b_{14} + D_{22}^2 b_{22} \\ &+ 2D_{22}D_{32}b_{23} + 2D_{22}D_{42}b_{24} + D_{32}^2 b_{33} + 2D_{32}D_{42}b_{34} + D_{42}^2 b_{44}, \\ \Lambda_{21} =& a_{41}^2 b_{11} + 2a_{41}a_{42}b_{12} + 2a_{41}a_{43}b_{13} + 2(a_2 - a_{11}a_{41} - a_{22}a_{41} - a_{33}a_{41})b_{14} \\ &+ a_{42}^2 b_{22} + 2a_{42}a_{43}b_{23} + 2(b_2 - a_{11}a_{42} - a_{22}a_{42} - a_{33}a_{42})b_{24} + a_{43}^2 b_{33} \\ &+ 2(c_2 - a_{11}a_{43} - a_{22}a_{43} - a_{33}a_{43})b_{34} \\ &+ (a_{11}^2 + 2a_{11}a_{22} + 2a_{11}a_{33} + a_{22}^2 + 2a_{22}a_{33} + a_{33}^2 + 2d_2)b_{44}, \\ \Lambda_{22} =& (a_2^2 - 2D_{14}a_{41})b_{11} + 2(a_2 b_2 - D_{14}a_{42} - D_{24}a_{41})b_{12} + 2(a_2 c_2 - D_{14}a_{43} \\ &- D_{34}a_{41})b_{13} + 2(D_{14}a_{11} + D_{14}a_{22} + D_{14}a_{33} - D_{44}a_{41} + a_2 d_2)b_{14} \\ &+ (b_2^2 - 2D_{24}a_{42})b_{22} + 2(b_2 c_2 - D_{24}a_{43} - D_{34}a_{42})b_{23} \\ &+ 2(D_{24}a_{11} + D_{24}a_{22} + D_{24}a_{33} - D_{44}a_{42} + b_2 d_2)b_{24} + (c_2^2 - 2D_{34}a_{43})b_{33}^2 \\ &+ 2(D_{34}a_{11} + D_{34}a_{22} + D_{34}a_{33} - D_{44}a_{43} + c_2 d_2)b_{34} \\ &+ (2D_{44}a_{11} + 2D_{44}a_{22} + 2D_{44}a_{33} + d_2^2)b_{44}, \\ \Lambda_{23} =& D_{14}^2 b_{11} + 2D_{14}D_{24}b_{12} + 2D_{14}D_{34}b_{13} + 2D_{14}D_{44}b_{14} + D_{24}^2 b_{22} \\ &+ 2D_{24}D_{34}b_{23} + 2D_{24}D_{44}b_{24} + D_{34}^2 b_{33} + 2D_{34}D_{44}b_{34} + D_{44}^2 b_{44}, \\ |D(w)|^2 =& (w^3 \mathrm{tr}A - \Omega_2 w)^2 + (\det A - w^2\Omega_1 + w^4)^2. \end{aligned}$$

The dominant frequencies of influenza in patches 1 and 2 are defined by the abscissa of the peaks of $P_1(w)$ and $P_2(w)$, respectively, and 2π divided by each dominant frequency gives the corresponding dominant period. The derivatives are as follows:

$$\frac{dP_1(w)}{dw} = \frac{Q(w)}{|D(w)|^4} = -4\pi w \frac{b_{22}w^{12} + h_5w^{10} + h_4w^8 + h_3w^6 + h_2w^4 + h_1w^2 + h_0}{|D(w)|^4},$$
$$\frac{d^2P_1(w)}{dw^2} = \frac{Q'(w)|D(w)|^4 - Q(w)(|D(w)|^4)'}{|D(w)|^8},$$

in which

$$\begin{aligned}
h_5 &= 2\,\Lambda_{11},\\
h_4 &= -b_{22}\,\Omega_1^2 - 2\,b_{22}\det A + 2\,b_{22}\,\mathrm{tr}A\,\Omega_2 - 2\,\Lambda_{11}\,\Omega_1 + \Lambda_{11}(\mathrm{tr}A)^2 + 3\,\Lambda_{12},\\
h_3 &= -2\,b_{22}\,\Omega_2^2 + 4\,b_{22}\,\Omega_1\det A + 2\,\Lambda_{12}(\mathrm{tr}A)^2 - 4\,\Lambda_{12}\,\Omega_1 + 4\,\Lambda_{13},\\
h_2 &= -3\,b_{22}(\det A)^2 - \Lambda_{11}\,\Omega_2^2 + 2\,\Lambda_{11}\,\Omega_1\det A + \Lambda_{12}\,\Omega_1^2\\
&\quad - 2\,\Lambda_{12}\,\mathrm{tr}A\,\Omega_2 + 2\,\Lambda_{12}\det A - 6\,\Lambda_{13}\,\Omega_1 + 3\,\Lambda_{13}(\mathrm{tr}A)^2,\\
h_1 &= -2\,\Lambda_{11}(\det A)^2 + 2\,\Lambda_{13}\,\Omega_1^2 - 4\,\Lambda_{13}\,\mathrm{tr}A\,\Omega_2 + 4\,\Lambda_{13}\det A,\\
h_0 &= -\Lambda_{12}(\det A)^2 - 2\,\Lambda_{13}\,\Omega_1\det A + \Lambda_{13}\,\Omega_2^2.
\end{aligned}$$

This peak point corresponds to a local maximum w_* of the function $P_1(w)$, which satisfies $Q(w_*) = 0$ and $Q'(w_*) < 0$. In essence, determining w_* amounts to finding the positive real roots of a sextic polynomial. Since no closed-form solution exists for general sextic equations, we must resort to numerical methods. The analysis of the peak for $P_2(w)$ is similar to that for $P_1(w)$ above. The presence of peak points in the PSD indicates the existence of stochastic quasi-cycle phenomena in the dynamical system. 2π divided by the abscissa of a maximum point ($2\pi/w_*$) corresponds to the dominant period of the dynamical system.

4. Results

In this section, we will use the annual influenza data from Beijing and Shanghai for 2004–2018 to fit our model and then discuss the influence of the dispersal rate on the dominant period of fluctuations in the infected population based on the above parameters.

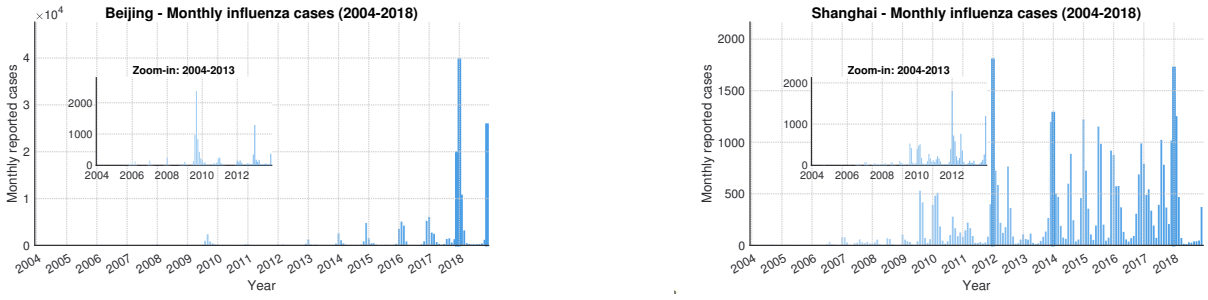
4.1. Influenza data and estimation of parameters

In this section, we take influenza as an example to fit the parameter values, so as to obtain the values used for the sensitivity analysis of the model parameters in the next subsection.

4.1.1. Influenza data

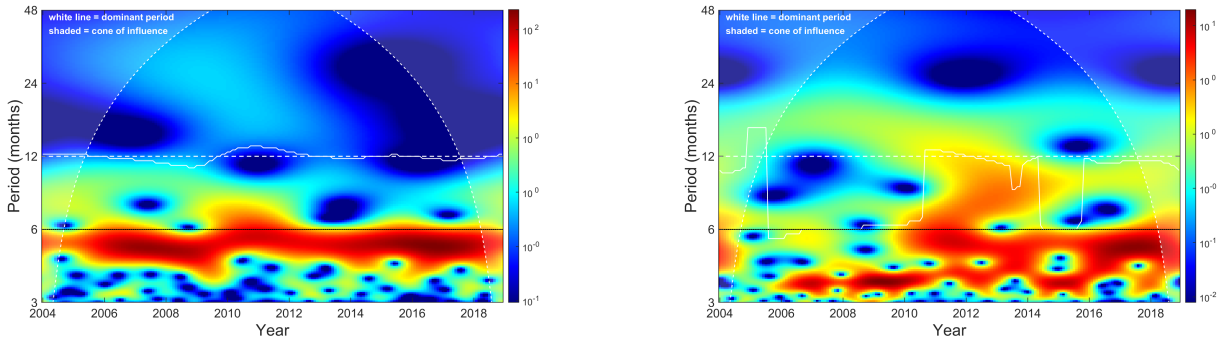
Figure 1 shows the monthly data for Beijing and Shanghai from 2004 to 2018. It can be seen that the influenza data from both cities exhibit a pronounced seasonal trend and are non-stationary. Wavelet analysis is then performed, with the results shown in Figure 2: The main period ridge for Beijing lies within 11.2–12.8 months, while that for Shanghai lies within 6–12.5 months. The dominant periods of both cities are shorter than one year, which is mainly attributed to the influence of environmental factors

such as temperature and humidity on influenza viruses. To fit the monthly data, the infection rate would have to be modeled as a periodic function; however, since this paper does not take environmental factors into account, we primarily use annual counts of new cases to fit the model parameters, consistent with our model's exclusion of seasonal forcing.



(a) Beijing **(b)** Shanghai

Figure 1. Monthly influenza data for Beijing and Shanghai.



(a) Beijing **(b)** Shanghai

Figure 2. Morlet wavelet power spectrum for Beijing and Shanghai.

4.1.2. Estimation of parameters

According to the 2019 statistical yearbooks of Beijing and Shanghai, the populations of Beijing and Shanghai in 2018 were 21.542 million and 24.2378 million, respectively, i.e., $N_1 = 21,542,000$ and $N_2 = 24,237,800$. The birth and death rates are $\mu_1 = 0.00597$ and $\mu_2 = 0.0077$. Since the birth rate is assumed to be equal to the death rate in the model, the parameter value is set to the median of the actual birth and death rates. The recovery rate is assumed to be $\gamma_1 = \gamma_2 = 26$ according to the mean duration of influenza (52 weeks/2 weeks).

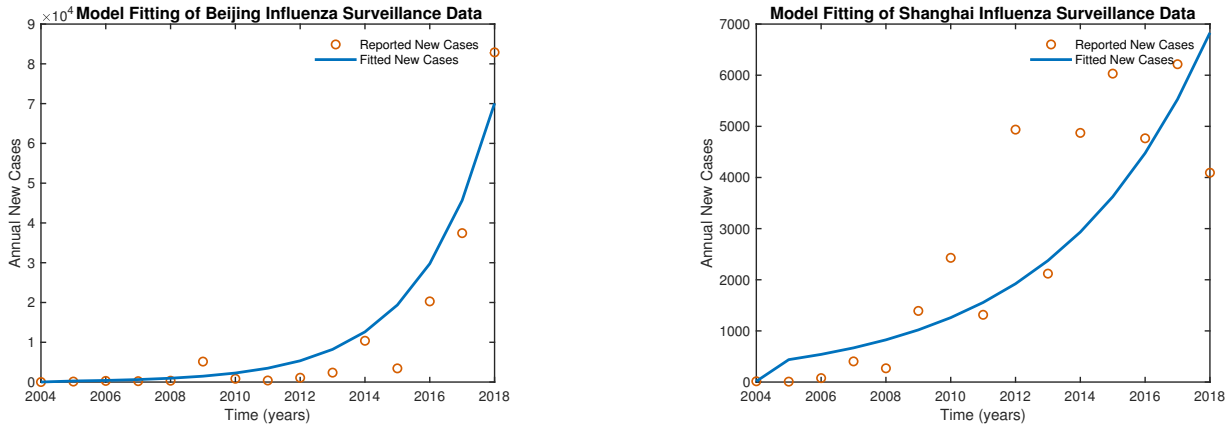
Optimal values for the other parameters are determined by applying the least-squares method. The least-squares objective function can be formulated as:

$$\min_{\theta} SS_{res}(\theta) = \sum_{j=1}^{2}\sum_{k=2}^{15}\left(Y_j^{obs}(k) - \int_{t_{k-1}}^{t_k} \beta_j \frac{S_j(t)I_j(t)}{N_j}\,\mathrm{d}t\right)^2,$$

in which θ=(d_{12}^S, d_{21}^S, β_1, β_2, d_{12}^I, d_{21}^I) denotes the parameter vector to be estimated, $Y_j^{obs}(k)$ represents

the number of new influenza cases in patch j in year $k + 2003$, and $\int_{t_{k-1}}^{t_k} \beta_j \frac{S_j(t)I_j(t)}{N_j} \mathrm{d}t$ represents the new cases generated by the model at time t_k in patch j. The lower and upper bounds of θ are set as follows: The lower bound is $\theta_l = (0.001, 0.001, 26.1, 26.1, 0.0001, 0.0001)$, and the upper bound is $\theta_u = (0.1, 0.1, 30, 30, 0.1, 0.1)$. A multi-start least-squares fitting approach is adopted, with the 2004 influenza data taken as the initial value at t_1. Then, 50 starting points are randomly selected within the upper and lower bounds of θ, and the quantitative goodness-of-fit index R^2 is calculated. In addition, Latin hypercube sampling is performed 1000 times within the bounds of θ to compute the partial rank correlation coefficients (PRCCs) of the different parameters. For each parameter θ we computed its profile likelihood by fixing θ on a grid around its MLE and reoptimizing the remaining five parameters and took the 95% profile confidence interval as the range over which Δ stays below the $\chi^2_{1,0.95} = 3.84$ threshold.

The simulation and fitting results, derived from the 2004–2018 influenza data for Beijing and Shanghai from the Chinese Center for Disease Control and Prevention, are presented in Figure 3. Table 2 lists all the corresponding parameter values. Given that the basic reproduction numbers for influenza in Beijing and Shanghai are both slightly above 1, the transmission rates are slightly higher than the recovery rates. For this parameter set, the quantitative goodness-of-fit indices for patch 1, patch 2, and the entire model are $R_1^2 = 0.9062$, $R_2^2 = 0.6606$, and $R^2 = 0.9103$, respectively. The corresponding PRCC results are shown in Figure 4. Since the PRCC values of d_{12}^I and d_{21}^I are less than 0.05, the model output is not sensitive to them over their admissible ranges, suggesting that they cannot be reliably estimated from the existing data. Figure 5 shows the profile likelihood curves for all six parameters. The profile for β_1 is a sharp, well-behaved valley that crosses the threshold on both sides, giving a narrow 95% CI of [26.41, 26.50], so this rate is tightly constrained by the data. In contrast, the profiles of β_2, d_{12}^S, d_{21}^S, d_{12}^I, and d_{21}^I remain essentially flat ($\Delta \approx 0$ throughout the scanned range) or rise monotonically to the edge of the range, indicating that their intervals are unbounded or one-sided and that the data carry little information in these directions. Since each curve is a marginal statement for a single parameter, these six intervals should not be combined into a joint confidence region.



(a) Beijing **(b)** Shanghai

Figure 3. Fitting results of influenza data for Beijing and Shanghai.

Table 2. Notation for model formulation and parameter values.

Parameters	Meaning	Value
N_1	the total population of patch 1	2.1542×10^7
N_2	the total population of patch 2	2.4238×10^7
γ_1	the recovery rate of I_1	26
γ_2	the recovery rate of I_2	26
u_1	the natural death rate and birth rate in patch 1	0.00597
u_2	the natural death rate and birth rate in patch 2	0.0077
β_1	the infection rate in patch 1	26.4356
β_2	the infection rate in patch 2	26.2190
d_{12}^S	the dispersal rate of susceptible individuals from patch 1 to patch 2	0.001
d_{21}^S	the dispersal rate of susceptible individuals from patch 2 to patch 1	0.1
d_{12}^I	the dispersal rate of infected individuals from patch 1 to patch 2	0.0001
d_{21}^I	the dispersal rate of infected individuals from patch 2 to patch 1	0.0001

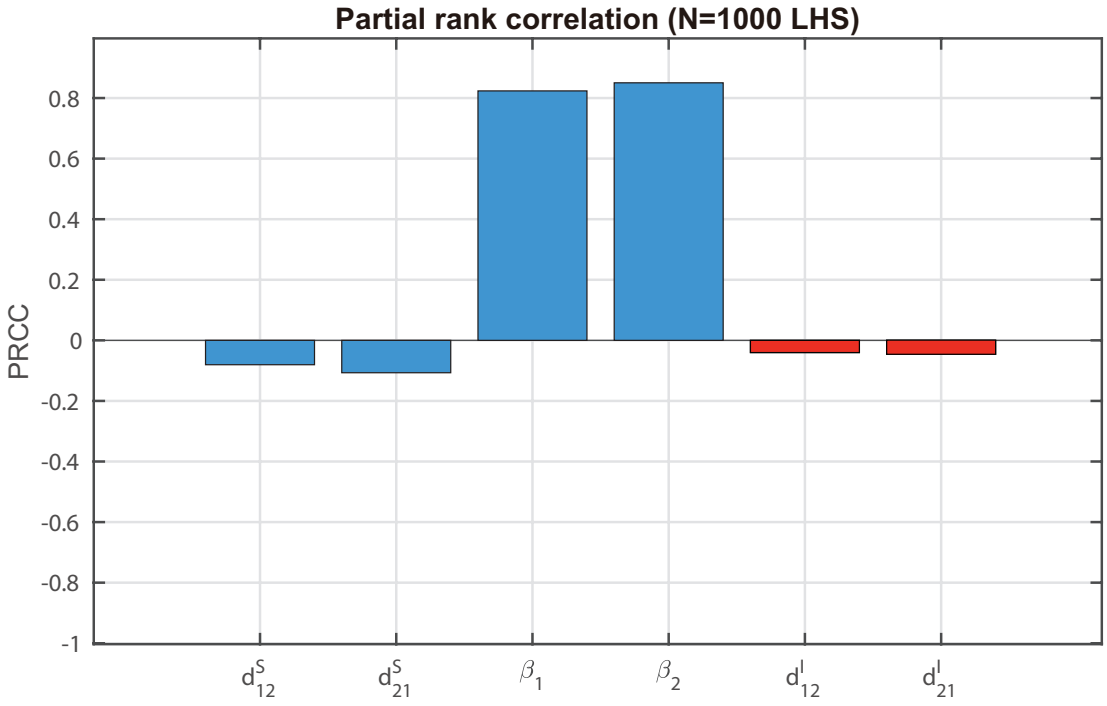


Figure 4. Partial rank correlation coefficients.

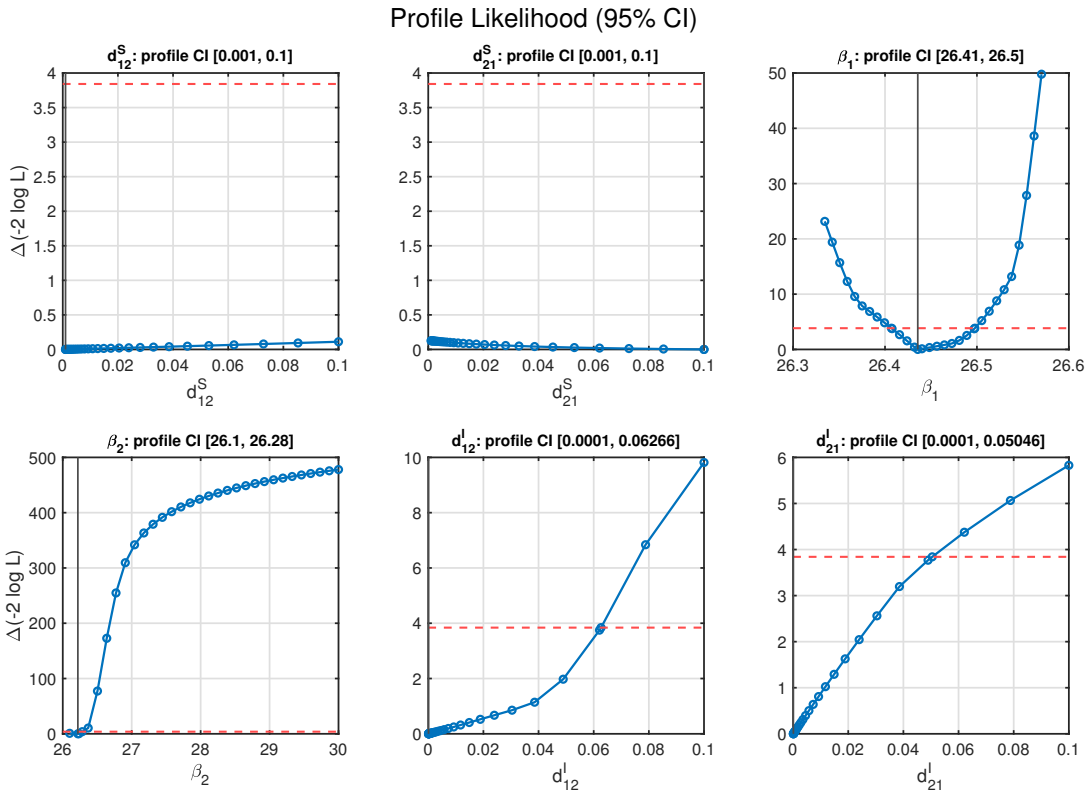


Figure 5. Profile likelihoods for the six fitted parameters. Blue curves: profile likelihood; red dashed line: $\chi^2_{1,0.95} = 3.84$ threshold; black vertical line: MLE. The labeled interval above each panel gives the 95% profile confidence interval.

For the profile likelihood analysis presented above, the influenza data are aggregated from monthly to annual resolution. This temporal aggregation reduces the number of observations by a factor of about 12 (from 180×2 to 15×2), corresponding to a loss of more than 90% of the data. However, this loss is not responsible for the limited identifiability of the dispersal parameters. If the aggregation were reversed and monthly resolution retained, i.e., if 12 times as many observations were available, the uncertainty in the transmission rates would decrease by a factor of only about 3.5 (standard errors scale as $\sqrt{12} \approx 3.5$). It should be noted that the above estimate of approximately 3.5 holds only under the simplifying assumption that observations are independent and equally informative. In dynamical epidemic models, temporal aggregation changes not only the number of observations but also the sensitivity of model parameters, the temporal correlation structure, and the information available for parameter estimation. This approximation should therefore be regarded as an order-of-magnitude indication; the realized change in standard errors is likely to be parameter-specific and may deviate appreciably from this estimate. Since β_1 and β_2 (boundary-related) are already well determined, this gain is of little consequence. By contrast, the current uncertainty in the dispersal parameters exceeds their entire admissible range by nearly three orders of magnitude. This suggests that the limited identifiability of these parameters arises mainly from structural features of the observation process itself: Influenza surveillance essentially records the number of infections at each patch, rather than the movement behavior of infected individuals, so that the influence of the dispersal rate on the

likelihood is largely smoothed out by the observation operator. This smoothing is a consequence of what is measured rather than of how often it is measured; increasing the temporal resolution therefore largely supplies additional realizations of the same aggregated quantity, rather than qualitatively new information about the dispersal process. From this perspective, even a reduction in standard errors proportional to the increase in sample size (about 3.5) would be far from sufficient to close a gap of nearly three orders of magnitude, and we therefore expect the dispersal parameters to remain poorly constrained at monthly resolution. We do not exclude the possibility that monthly data could in principle improve their identifiability; the above expectation remains to be tested by formal model fitting and identifiability analysis at monthly resolution, which we identify as a direction for future work. Since this paper mainly focuses on the effect of the dispersal rates on the stochastic quasi-cycles of the epidemic, while the dispersal rates of influenza are unidentifiable as shown above, the analysis in the next section will be based on this set of parameters, and a theoretical sensitivity analysis of the model will be carried out.

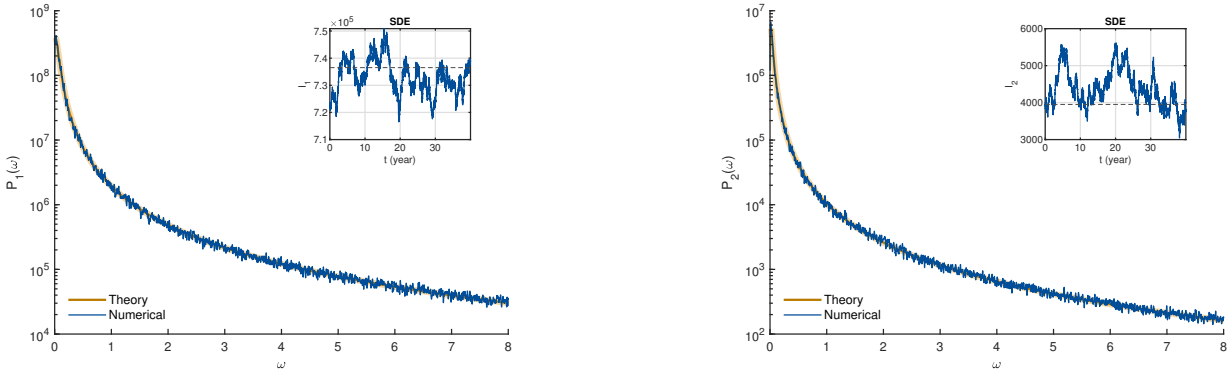
4.2. Theoretical sensitivity analysis of the dispersal rate

Using the fitted parameters above, we will now focus on examining the effect of the diffusion rate on the power spectra $P_1(w)$ and $P_2(w)$. By fixing the other parameters, we find that R_0 is always greater than 1 when the diffusion rate is positive. Therefore, in the following discussion, the parameter region is set to (0,0.5). The dominant frequencies of fluctuations in the infected populations in patches 1 and 2 are defined by the abscissas of the extrema of $P_1(w)$ and $P_2(w)$, respectively, and 2π multiplied by the reciprocal of each frequency gives the corresponding dominant period. Therefore, we first address the question of whether such an extremum point, and hence a dominant period, exists within the chosen parameter region. Subsequently, if it does, we will explore the relationship between the diffusion rate and the dominant period.

Figures 7–9 clearly show the distribution of maximum points of $P_1(w)$ and $P_2(w)$ in different parameter planes. A region with no maximum signifies that the diffusion-driven oscillations in the infected population do not exhibit stochastic quasi-cycles. Conversely, the presence of a maximum allows for the determination of the dominant period of these oscillations. Thus, with the current fitted parameters, infectious disease in patch 1 and patch 2 does not show a dominant period in our fitted stochastic model. The plots of the theoretical results and the numerical simulations of $P_1(w)$ and $P_2(w)$ in Figure 6 also verify this conclusion. In Figure 7, $P_1(w)$ ($P_2(w)$) has no dominant period for any d_{21}^I between 0 and 0.5 when $d_{12}^I \in (0, 0.0071)$ ($d_{12}^I \in (0, 0.006)$), or when $d_{12}^I \in (0.41, 0.5)$ ($d_{12}^I \in (0.43, 0.5)$) and d_{21}^I is very small. Figure 8 presents the distribution of the number of local maxima of $P_1(w)$ and $P_2(w)$ over the parameter plane (d_{12}^S, d_{12}^I) or (d_{21}^S, d_{21}^I). The four subplots demonstrate that, when the other parameters are held fixed, the stochastic quasi-cycle behavior in both patches emerges only when the diffusion rate of susceptible individuals, d_{12}^S or d_{21}^S, lies within a very small range. Figure 9 mainly investigates the combined effect of the transmission rates β_1 and β_2 and the diffusion rates of infected individuals d_{12}^I and d_{21}^I on the number of local maxima in the two patches. In Figure 9(c), β_2 and d_{21}^I have no effect on the dominant frequency of patch 1, possibly because the number of infected individuals in patch 2 is relatively small compared with that in patch 1. In Figure 9(a), in the upper-left and lower-right regions of the parameter plane (d_{12}^I, β_1), there are no local maxima and thus no effect on the dominant frequency of patch 1, while the dominant frequency exists in the remaining regions. In Figure 9(b), in the same parameter plane as in Figure 9(a), the upper-right and lower-right

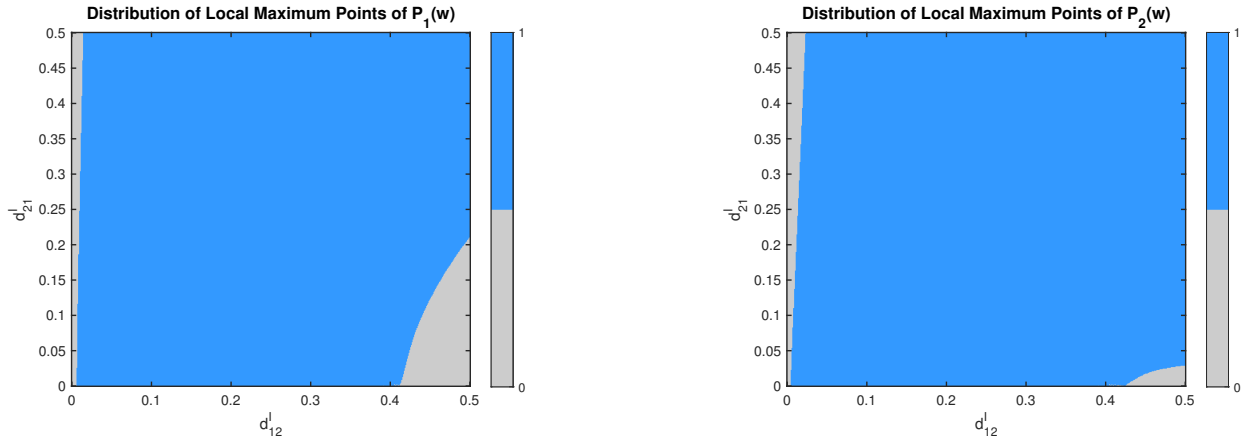
regions have no effect on the dominant frequency of patch 2, while the dominant frequency exists in the remaining regions. In Figure 9(d), in the lower-right region of the parameter plane (d_{21}^I, β_2), except for a cone-shaped region, there are no local maxima, and thus no effect on the dominant frequency of patch 2.

Figure 10 focuses on the dominant frequency corresponding to the region with one maximum, examining the relationship between the diffusion rates d_{21}^I and d_{12}^I and the dominant period. As shown in Figure 10(a), the relationship between the dominant frequency of infectious disease in patch 1 and the diffusion rate is non-monotonic. When d_{12}^I is held constant, the dominant frequency (and thus the dominant period) first increases (decreases) and then decreases (increases) as d_{21}^I increases. Similarly, when d_{21}^I is held constant, the dominant frequency (and thus the dominant period) first increases (decreases) and then decreases (increases) as d_{12}^I increases. The relationship between the dominant period and parameters d_{12}^I and d_{21}^I in patch 2 in Figure 10(b) is similar to that in Figure 10(a). Figure 11 mainly investigates the combined effect of the transmission rates β_1 and β_2 and the diffusion rates of infected individuals d_{12}^I and d_{21}^I on the dominant frequencies of the two patches. In Figure 11(a), when the diffusion rate of infected individuals d_{12}^I is fixed, the dominant frequency of patch 1 increases with the transmission rate β_1; when β_1 is fixed, the variation of the dominant frequency with the diffusion rate of infected individuals d_{12}^I exhibits a distinct boundary. In Figure 11(b), when the transmission rate β_1 is fixed, the dominant frequency of patch 2 increases as the diffusion rate of infected individuals d_{12}^I increases. In Figure 11(c), the dominant frequency in the upper part of the parameter plane (d_{21}^I, β_2) is relatively small and changes little, while in the lower-right region of the parameter plane, the variation pattern of the dominant frequency is similar to that in Figure 11(a).



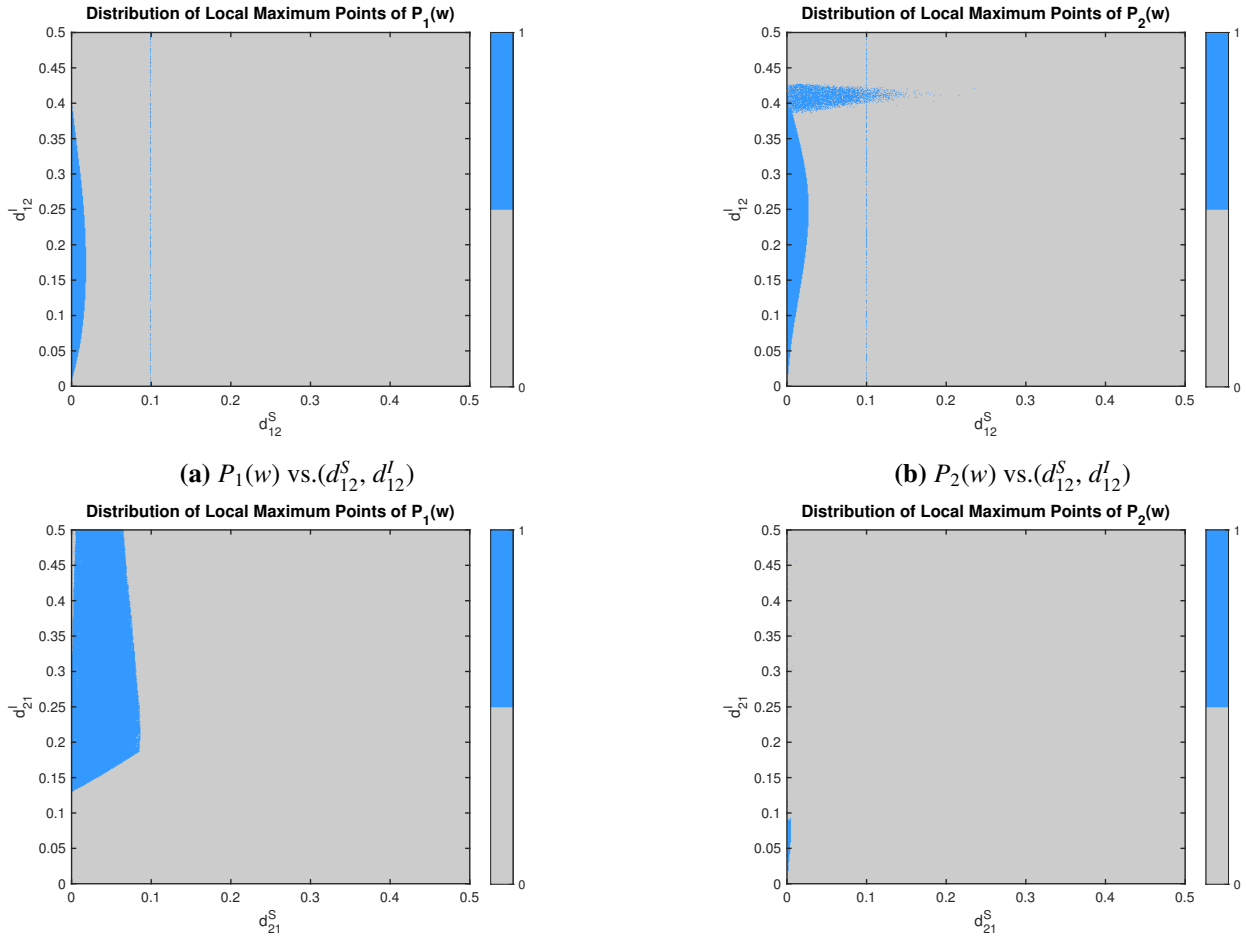
(a) $P_1(w)$ **(b)** $P_2(w)$

Figure 6. Comparison of the theoretical power spectrum with the numerical simulation results.



(a) $P_1(w)$ vs.(d_{12}^I, d_{21}^I) **(b)** $P_2(w)$ vs.(d_{12}^I, d_{21}^I)

Figure 7. Distribution of maximum points of $P_1(w)$ and $P_2(w)$ in the (d_{12}^I, d_{21}^I) parameter plane. Gray: no local maximum; blue: one local maximum (a dominant peak is present).



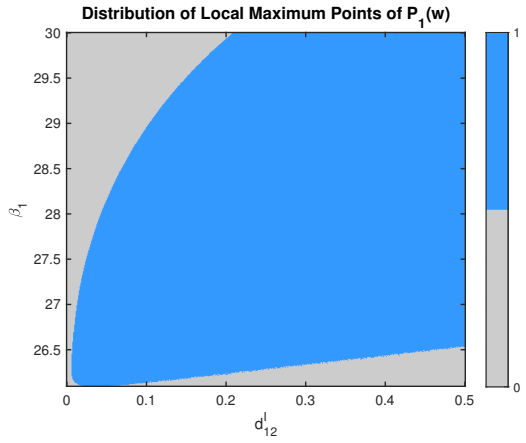
(a) $P_1(w)$ vs.(d_{12}^S, d_{12}^I)

(b) $P_2(w)$ vs.(d_{12}^S, d_{12}^I)

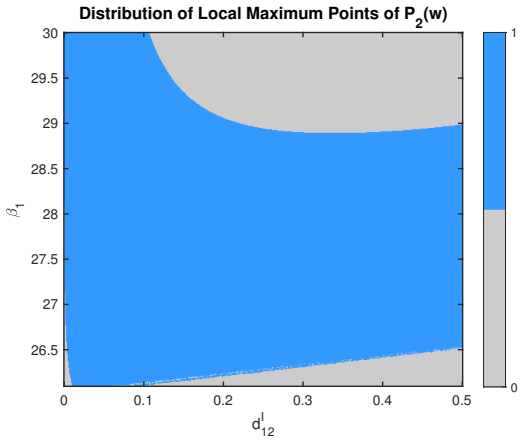
(c) $P_1(w)$ vs.(d_{21}^S, d_{21}^I)

(d) $P_2(w)$ vs.(d_{21}^S, d_{21}^I)

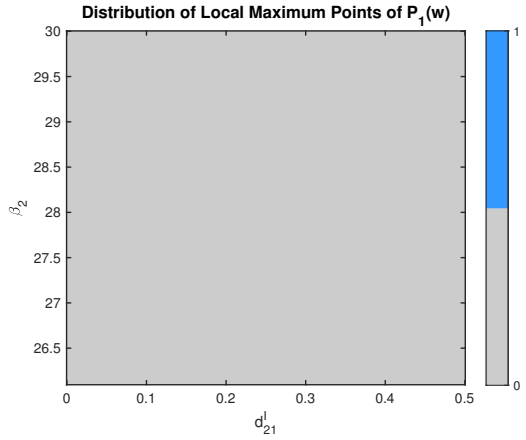
Figure 8. Distribution of maximum points of $P_1(w)$ and $P_2(w)$ in the (d_{12}^S, d_{12}^I) or (d_{21}^S, d_{21}^I) parameter plane. Gray: no local maximum; blue: one local maximum (a dominant peak is present).



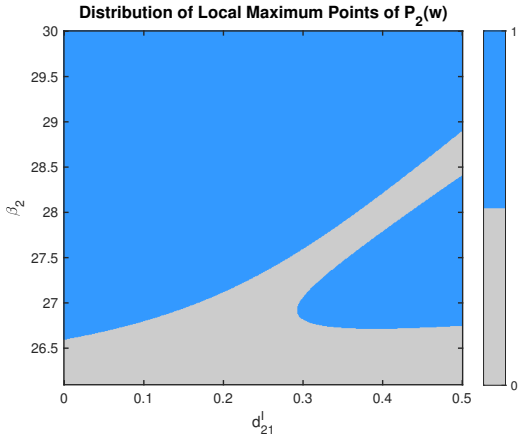
(a) $P_1(w)$ vs.(d_{12}^I, β_1)



(b) $P_2(w)$ vs.(d_{12}^I, β_1)

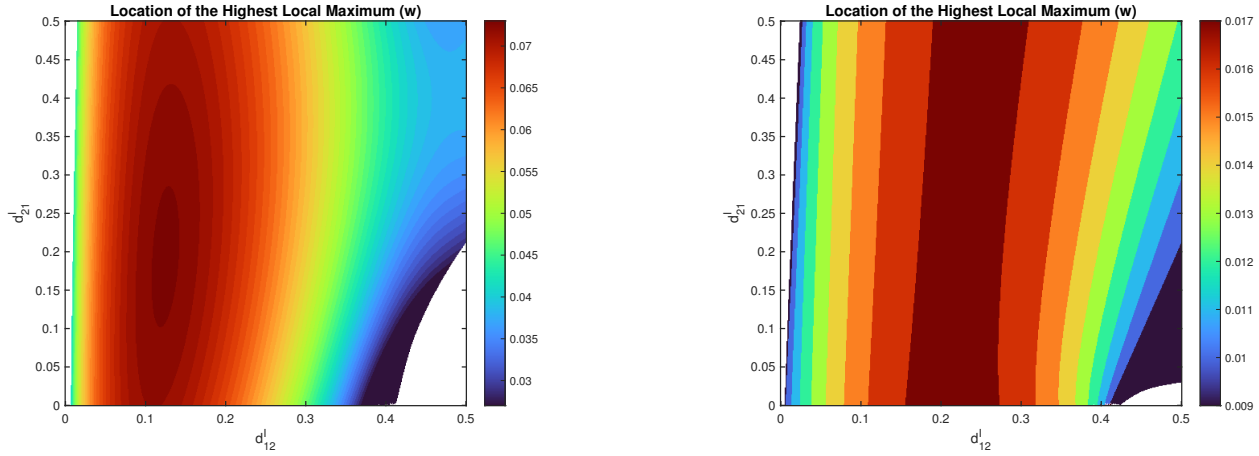


(c) $P_1(w)$ vs.(d_{21}^I, β_2)



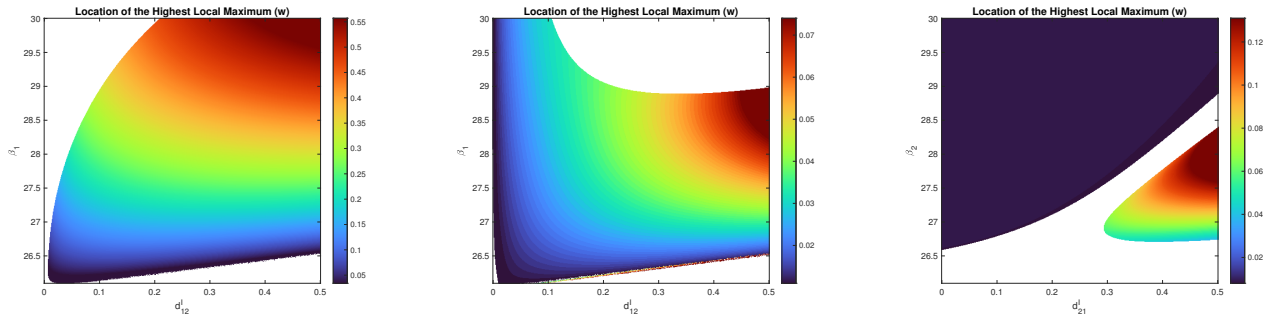
(d) $P_2(w)$ vs.(d_{21}^I, β_2)

Figure 9. Distribution of maximum points of $P_1(w)$ and $P_2(w)$ in the (d_{12}^I, β_1) or (d_{21}^I, β_2) parameter plane. Gray: no local maximum; blue: one local maximum (a dominant peak is present).



(a) $P_1(w)$ vs.(d_{12}^I, d_{21}^I) **(b)** $P_2(w)$ vs.(d_{12}^I, d_{21}^I)

Figure 10. Location of the abscissa (w) for $P_1(w)$ and $P_2(w)$ in the (d_{12}^I, d_{21}^I) parameter plane with one maximum. In each panel, warmer colors (red/orange) indicate larger ω and cooler colors (blue/purple) indicate smaller ω; the color bar gives the corresponding values. The two panels use different color scales, so colors are not directly comparable between Figure 10(a) and Figure 10(b). White regions indicate parameter combinations for which no local maximum was detected; these are left blank, carry no value, and correspond to the gray regions in Figure 7.



(a) $P_1(w)$ vs.(d_{12}^I, β_1) **(b)** $P_2(w)$ vs.(d_{12}^I, β_1) **(c)** $P_2(w)$ vs.(d_{21}^I, β_2)

Figure 11. Location of the abscissa (w) for $P_1(w)$ and $P_2(w)$ in the (d_{12}^I, β_1) or (d_{21}^I, β_2) parameter plane with one maximum. In each panel, warmer colors (red/orange) indicate larger ω and cooler colors (blue/purple) indicate smaller ω; the color bar gives the corresponding values. The three panels use different color scales, so colors are not directly comparable between Figure 11(a), Figure 11(b), and Figure 11(c). White regions indicate parameter combinations for which no local maximum was detected; these are left blank, carry no value, and correspond to the gray regions in Figure 9(a), Figure 9(b), and Figure 9(d).

5. Conclusions and discussion

In this study, we focus on the relationship between the population diffusion rate and the dominant period of infectious disease under the condition $R_0 > 1$. The model parameters are fitted by using influenza data from Beijing and Shanghai (2004–2018) and then used to investigate the relationship between the diffusion rate and the dominant period. Our analysis within the designated parameter space $d_{12}^I * d_{21}^I \in (0, 0.5) * (0, 0.5)$ reveals that a dominant period exists across most of this space, with the exception of regions where the diffusion rate is very small. The diffusion rate of the susceptible is affected by that of the infected, and quasi-periodicity can only emerge within a small parameter region. The synergistic effect of the transmission rate and the diffusion rate of the infected on the dominant frequency is parameter-dependent, with a clear frequency boundary appearing in certain parameter regions. Contrary to the common assumption that a higher diffusion rate leads to a shorter dominant period, our numerical results demonstrate a distinct nonlinear relationship in certain parameter regions. Specifically, the dominant period initially decreases as the diffusion rate increases, but subsequently begins to increase. These findings provide a theoretical framework for understanding the relationship between the diffusion rate and the dominant period of infectious disease, yet since the sextic equation has no explicit solution, the above results depend on the model structure and the parameter values.

Given the substantial computational challenges posed by high-dimensional systems, this study is limited to the case of population movement between two patches. Future work will leverage advanced algorithms to investigate the dominant period in more complex multi-patch or metapopulation models. The mobility rate of infected individuals has low identifiability; future studies may use high-precision mobility data to enhance parameter identifiability. Environmental factors are not considered in the transmission rate; incorporating periodic factors in future work could better capture the real-world patterns of epidemic spread. We also note that constant population sizes were assumed over the entire study period, whereas both cities underwent considerable demographic changes during 2004–2018. This simplification may affect the absolute scale of estimated incidence and potentially bias the estimated transmission rates to some extent. Future studies incorporating time-varying demographic data are warranted to further refine the parameter estimates.

Author contributions

Hong Yang conceived the idea, drafted the manuscript, and performed parameter fitting. Fenfen Zhang participated in the discussion and secured the funding. All authors have read and approved the final version of the manuscript for publication.

Use of Generative-AI tools declaration

The authors declare they have not used Artificial Intelligence (AI) tools in the creation of this article.

Acknowledgments

This work is supported by the Foundation for Young Scholars of Shanxi Province, China (202303021212249, 202403021222271, 202503021212244), the National Natural Science Foundation

of China (12501691, 12601956).

Conflict of interest

The authors declare that they have no known competing financial interests or personal relationships that could have appeared to influence the work reported in this paper.

References

1. S. P. de Jong, A. J. Conlan, A. X. Han, C. A. Russell, Competition between transmission lineages mediated by human mobility shapes seasonal influenza epidemics in the US, *Nat. Commun.*, **16** (2025), 4605. https://doi.org/10.1038/s41467-025-59757-4
2. S. Pei, S. Kandula, W. Yang, J. Shaman, Forecasting the spatial transmission of influenza in the United States, *P. Natl. A. Sci. USA*, **115** (2018), 2752–2757. https://doi.org/10.1073/pnas.1708856115
3. P. Agarwal, J. J. Nieto, D. F. M. Torres, *Mathematical analysis of infectious diseases*, Academic Press, Cambridge, MA, 2022.
4. A. ul Rehman, R. Singh, P. Agarwal, Modeling, analysis and prediction of new variants of Covid-19 and dengue co-infection on complex network, *Chaos Soliton. Fract.*, **150** (2021), 111008. https://doi.org/10.1016/j.chaos.2021.111008
5. S. Chowdhury, J. Chowdhury, S. F. Ahmed, P. Agarwal, I. A. Badruddin, S. Kamangar, Mathematical modelling of COVID-19 disease dynamics: Interaction between immune system and SARS-CoV-2 within host, *AIMS Math.*, **7** (2022), 2618–2633. https://doi.org/10.3934/math.2022147
6. C. Castillo-Chavez, A. A. Yakubu, Dispersal, disease and life-history evolution, *Math. Biosci.*, **173** (2001), 35–53. https://doi.org/10.1016/S0025-5564(01)00065-7
7. F. Simini, M. C. González, A. Maritan, A. Barabási, A universal model for mobility and migration patterns, *Nature*, **484** (2012), 96–100. https://doi.org/10.1038/nature10856
8. D. Citron, C. Guerra, A. Dolgert, S. Wu, J. Henry, D. Smith, et al., Comparing metapopulation dynamics of infectious diseases under different models of human movement, *P. Natl. A. Sci. USA*, **118** (2021). https://doi.org/10.1073/pnas.2007488118
9. W. Wang, G. Mulone, Threshold of disease transmission in a patch environment, *J. Math. Anal. Appl.*, **285** (2003), 321–335. https://doi.org/10.1016/S0022-247X(03)00428-1
10. S. Chen, J. Shi, Z. Shuai, Y. Wu, Asymptotic profiles of the steady states for an SIS epidemic patch model with asymmetric connectivity matrix, *J. Math. Biol.*, **80** (2020), 2327–2361. https://doi.org/10.1007/s00285-020-01497-8
11. D. Ayabina, H. Sevil, A. Kleczkowski, M. G. M. Gomes, A note on metapopulation models, *J. Theor. Biol.*, 2025, 112213. https://doi.org/10.1016/j.jtbi.2025.112213
12. A. L. Krause, L. Kurowski, K. Yawar, R. A. Van Gorder, Stochastic epidemic metapopulation models on networks: SIS dynamics and control strategies, *J. Theor. Biol.*, **449** (2018), 35–52. https://doi.org/10.1016/j.jtbi.2018.04.023

13. H. Yu, W. J. Alonso, L. Feng, Y. Tan, Y. Shu, W. Yang, et al., Characterization of regional influenza seasonality patterns in China and implications for vaccination strategies: Spatio-temporal modeling of surveillance data, *PLOS Med.*, **10** (2013), e1001552. https://doi.org/10.1371/journal.pmed.1001552
14. X. Si, *Weather variability, socio-environmental factors and seasonal influenza transmission in mainland China: Spatiotemporal analyses*, PhD thesis, Queensland University of Technology, 2025.
15. C. Liu, H. Liu, X. Zhu, Z. Gangji, Q. Zhang, Y. Wei, Regional and seasonal analysis of influenza epidemics: A mathematical modeling study of 15 provinces in China, *Int. J. Biomath.*, 2025, 2550099. https://doi.org/10.1142/S1793524525500998
16. C. Andreu-Vilarroig, G. González-Parra, R. J. Villanueva, Mathematical modeling of influenza dynamics: Integrating seasonality and gradual waning immunity, *Bull. Math. Biol.*, **87** (2025), 75. https://doi.org/10.1007/s11538-025-01454-w
17. K. M. Mohammad, A. A. Akhi, M. Kamrujjaman, Bifurcation analysis of an influenza A (H1N1) model with treatment and vaccination, *PloS One*, **20** (2025), e0315280. https://doi.org/10.1371/journal.pone.0315280
18. X. Zhang, X. Zhang, D. Jiang, A study of a seasonal influenza model in deterministic and stochastic environments, *J. Nonlinear Sci.*, **35** (2025), 37. https://doi.org/10.1007/s00332-025-10132-z
19. R. Saadeh, A. A. Shokeralla, N. Al-Kuleab, W. S. Hamad, M. Ali, M. A. Abdoon, et al., Stochastic modelling of seasonal influenza dynamics: Integrating random perturbations and behavioural factors, *Eur. J. Pure Appl. Math.*, **18** (2025), 6379–6379. https://doi.org/10.29020/nybg.ejpam.v18i3.6379
20. Y. Tan, R. Yao, Dynamics of an influenza epidemic model incorporating immune boosting and Ornstein–Uhlenbeck process, *Chaos Soliton. Fract.*, **188** (2024), 115446. https://doi.org/10.1016/j.chaos.2024.115446
21. J. Chaffee, R. Kuske, The effect of loss of immunity on noise-induced sustained oscillations in epidemics, *Bull. Math. Biol.*, **73** (2011), 2552–2574. https://doi.org/10.1007/s11538-011-9635-7
22. P. D. Pra, E. Marini, Noise-induced oscillations for the mean-field dissipative contact process, *Electron. J. Probab.*, **30** (2025), 1–31. https://doi.org/10.1214/25-EJP1295
23. A. Hamdouni, M. E. Zidan, A. B. Mabrouk, M. Guettari, A wavelet time-frequency analysis of pandemic dynamics and impacts-Covid-19 case study, *Int. J. Biomath.*, 2025. https://doi.org/10.1142/S1793524525500561
24. C. Mills, F. Falconi-Agapito, J. P. Carrera, C. Munayco, M. U. Kraemer, C. A. Donnelly, Multi-model approach to understand and predict past and future dengue epidemic dynamics, *Roy. Soc. Open Sci.*, **12** (2025), 241870. https://doi.org/10.1098/rsos.241870
25. D. K. C. Vijaya, P. D. Gowda, B. Hadimani, A numerical study on the dynamics of SIR epidemic model through Genocchi wavelet collocation method, *Sci. Rep.*, **15** (2025), 9780. https://doi.org/10.1038/s41598-025-93820-w
26. R. H. Wang, Z. Jin, Q. X. Liu, J. V. D. Koppel, D. Alonso, A simple stochastic model with environmental transmission explains multi-year periodicity in outbreaks of avian flu, *PLoS One*, **7** (2012), e28873. https://doi.org/10.1371/journal.pone.0028873

27. H. Yang, Z. Jin, A stochastic model explains the periodicity phenomenon of influenza on network, *Sci. Rep.*, **11** (2021), 20996. https://doi.org/10.1038/s41598-021-00260-3

28. O. Diekmann, J. A. P. Heesterbeek, J. A. J. Metz, On the definition and the computation of the basic reproduction ratio r 0 in models for infectious diseases in heterogeneous populations, *J. Math. Biol.*, **28** (1990), 365–382.

29. P. Van den Driessche, J. Watmough, Reproduction numbers and sub-threshold endemic equilibria for compartmental models of disease transmission, *Math. Biosci.*, **180** (2002), 29–48. https://doi.org/10.1016/S0025-5564(02)00108-6



AIMS Press

© 2026 the Author(s), licensee AIMS Press. This is an open access article distributed under the terms of the Creative Commons Attribution License (https://creativecommons.org/licenses/by/4.0)